Journal of Membrane Science 453 (2014) 240–252

Contents lists available at ScienceDirect

Journal of Membrane Science

journal homepage: www.elsevier.com/locate/memsci

Osmotic equilibrium in the forward osmosis process: Modelling, experiments and implications for process performance

Sherub Phuntsho [a], Seungkwan Hong [b], Menachem Elimelech [c], Ho Kyong Shon [a,*]

[a] School of Civil and Environmental Engineering, University of Technology, Sydney (UTS), Post Box 129, Broadway, NSW 2007, Australia
[b] School of Civil, Environmental & Architectural Engineering, Korea University, 1, 5-ka, Anam-Dong, Sungbuk-Gu, Seoul 136-713, Republic of Korea
[c] Department of Chemical and Environmental Engineering, Yale University, P.O. Box 208286, New Haven, CT 06520-8286, USA

ARTICLE INFO

Article history:
Received 5 August 2013
Received in revised form
5 November 2013
Accepted 8 November 2013
Available online 19 November 2013

Keywords:
Forward osmosis
Osmotic equilibrium
Desalination
Crossflow direction
Modelling

ABSTRACT

Forward osmosis (FO) has gained significant research interest due to the wide range of potential applications in desalination and wastewater reuse. However, the FO process being concentration (osmosis) driven has its own intrinsic limitations. Net transfer of water across the membrane occurs until the point of osmotic equilibrium between the draw solution (DS) and the feed solution (FS). Without external intervention, it is impossible to dilute the DS beyond the point of osmotic equilibrium. In this study, the concept of osmotic equilibrium in the FO process is introduced by simulating conditions in a plate-and-frame FO membrane module using established mass transport models. The simulations evaluated the influence of various operating parameters on process performance, assessed in terms of water flux, feed recovery rate and the final concentration of the diluted DS. The counter-current crossflow mode of operation has been observed to be advantageous because it can achieve higher module average water flux, higher feed water recovery rates and higher DS final dilution. Based on the osmotic equilibrium concept and mass balance analysis, a modified equation for the water extraction capacity of a draw solute has been proposed. This study underscores the need for process optimisation for large-scale FO operations.

1. Introduction

Forward osmosis (FO) is an osmotically driven membrane process that has lately drawn research interest for several applications, notably desalination for potable [1,2] and non-potable [3–5] purposes, water treatment [6], wastewater treatment [7,8], pharmaceutical applications [6], food processing [9], osmotic power generation [10–13], and pre-treatment for RO desalination [14–16]. The research on FO is mainly driven by the need to lower the energy and chemical demands of conventional salt-rejecting membrane processes.

In FO, a concentrated draw solution (DS) is used to draw water through the membrane from a feed solution (FS). The concentration or osmotic pressure difference between the two solutions acts as the driving force for water permeation through the membrane. The FO process, therefore, does not require an applied hydraulic pressure like the traditional reverse osmosis (RO) process. The water permeating from the FS finally dilutes the concentrated DS, which exits the membrane module as a diluted DS. Depending on the final end use of the product water, the diluted DS may be required to undergo some post-treatment process to separate draw solutes from the pure water or in some cases the diluted DS may be used directly.

Although numerous works have indicated the potential of FO as a low energy desalination process [2,3,6,11,15,17], none have identified or demonstrated the osmotic equilibrium as the ultimate end of the FO process nor how this phenomenon could act as a major process limitation for full-scale applications. The FO process is driven by the concentration or osmotic pressure difference between the FS and DS. During the FO process, the permeating water dilutes the DS, but only to a certain extent, i.e., until an osmotic equilibrium is reached between the DS and the FS. At this point, the osmotic pressure driving force vanishes. Osmotic equilibrium, therefore, determines the final concentration of the diluted DS, which has direct implications for the end use of the final product water. For example, in the case of potable water application, the draw solute must be separated from the pure water and then recycled for reuse. The energy required for the post-treatment of the diluted DS will therefore depend on the concentration of the diluted DS. If the diluted DS is intended for direct use, such as fertigation, the final fertiliser concentration must meet the water quality standard for nutrient applications [18,19].

The net transfer of water across the membrane vanishes when an osmotic equilibrium is established between the feed and draw

* Corresponding author. Tel.: +61 2 9514 2629; fax: +61 2 9514 2633.
E-mail addresses: Hokyong.Shon-1@uts.edu.au, shonhokyong@yahoo.co.kr (H.K. Shon).

0376-7388/$ - see front matter © 2013 Elsevier B.V. All rights reserved.
http://dx.doi.org/10.1016/j.memsci.2013.11.009

solutions. Osmotic equilibrium is therefore one of the most significant points occurring along the length of the channel in an FO membrane module. In this study, we introduce for the first time, the concept of osmotic equilibrium, and analyse its impact on the FO process performance through a one-dimensional plug flow simulation in a plate-and-frame FO membrane module under co-current and counter-current crossflow directions. The influences of various process parameters are simulated to evaluate their impact in terms of three important indicators: module average water flux, feed water recovery rate and diluted DS final concentration. The simulation results are then used to explain why counter-current crossflow would be more advantageous than co-current crossflow mode in FO operation. Finally, the implication of crossflow directions on the water extraction capacity of draw solutes is demonstrated.

2. Modelling

2.1. Water flux in the FO process

Osmosis is the natural diffusion of water through a semi-permeable membrane driven by the concentration or osmotic pressure difference. The osmotic pressure equation developed by van't Hoff [20] is widely used:

$$\pi = n\,C\,R\,T \tag{1}$$

where n is the van't Hoff factor (accounts for the number of individual particles of a compound dissolved in the solution, for example $n=2$ for NaCl, $n=1$ for glucose), C is the molar concentration (molarity) of the solution, R is the gas constant ($R=0.0821$ L atm mol^{-1} K^{-1}) and T is the absolute temperature (in K) of the solution. The van't Hoff equation is, however, applicable only to dilute solutions [21].

In the FO desalination process, water from the feed moves towards the highly concentrated DS (leaving behind the solutes) due to the osmotic pressure gradient, when a semipermeable membrane separates the two solutions. The water flux (J_w) in the FO process is given by [6,22]

$$J_w = A\,\sigma[\pi_D - \pi_F] \tag{2}$$

where A is the membrane pure water permeability coefficient, σ is the reflection coefficient, and π_D and π_F are the osmotic pressures of the DS and FS, respectively. For most applications where the salt rejection is relatively high, like in this study, the reflection coefficient can be assumed unity.

Eq. (2) is valid only for dilute solutions and when concentration polarisation phenomena are neglected. However, concentration polarisation phenomena play a critical role in FO process and therefore must be accounted for as described in the following sections.

2.2. Concentrative external concentration polarisation (ECP) and dilutive internal concentration polarisation (ICP)

The presence of two independent solutions on each side of the membrane results in two different types of CP: concentrative CP on the membrane surface facing the FS and dilutive CP on the membrane surface facing the DS. Since the dense synthetic polymeric membranes are usually asymmetric in design (thin active layer sitting on the top of the porous support layer), CP effects can occur either on the active layer (external CP or ECP) and inside the support layer (internal CP or ICP). For a process operated in FO mode (FS facing the membrane active layer and DS facing the porous support layer), CP phenomena involve concentrative ECP and dilutive ICP.

Concentrative ECP is a well-documented phenomenon in pressure-driven membrane processes [23,24]. A similar phenomenon occurs in the FO process on the feed side facing the active layer of the FO membrane. The concentration or the osmotic pressure of the feed on the membrane active layer ($\pi_{F,m}$) is described by the following equation [25]:

$$\pi_{F,m} = \pi_{F,b}\exp\left(\frac{J_w}{k}\right) \tag{3}$$

where $\pi_{F,b}$ is the bulk osmotic pressure of the FS and k_F the mass transfer coefficient of the feed side boundary layer. The latter is given by the following relationship:

$$k_F = \frac{Sh\,D_F}{d_h} \tag{4}$$

Here Sh refers to the Sherwood number, D_F the diffusion coefficient of the feed solute and d_h the hydraulic diameter of the feed channel. The Sherwood number is given by the following relationship based on the flow conditions in the channel:

$$Sh = 1.85\left(Re\,Sc\frac{d_h}{L}\right)^{0.33} \quad \text{(laminar flow)} \tag{5}$$

$$Sh = 0.04\,Re^{0.75}Sc^{0.33} \quad \text{(turbulent flow)} \tag{6}$$

Here, Re is the Reynolds number, Sc the Schmidt number and L the length of the channel. The Schmidt number (Sc) can be determined by the following relationship:

$$Sc = \frac{\nu}{D_F} = \frac{\mu}{\rho\,D_F} \tag{7}$$

where ν is the kinematic viscosity of the solution, ρ the solution density and μ the dynamic viscosity.

Dilutive ICP occurs on the other side of the membrane (i.e., the support layer) facing the DS and inside the membrane support layer. The convective flux from the feed displaces and drags the draw solutes away from the membrane active layer interface. This decreases the concentration of the draw solutes near the active layer thereby reducing the effective driving force. The osmotic pressure inside the porous support layer ($\pi_{D,i}$) near the active layer membrane interface is given by the following equation [25]:

$$\pi_{D,i} = \pi_{D,b}\exp(-J_w K_D) \tag{8}$$

where and K_D is the solute resistivity for diffusion of draw solutes within the porous support layer and is defined as:

$$K_D = \frac{t\tau}{D_D\,\varepsilon} \tag{9}$$

where t, τ and ε are the thickness, tortuosity and porosity of the support layer, respectively. While the values of t, τ and ε are constant for a particular membrane, the value of D_D is likely to vary depending on the types of draw solutes used and the concentration. K_D is therefore a measure of effectiveness of the solute to diffuse into and out of the support layer and hence is a parameter that measures the severity of ICP in the FO process. The value of K_D can be determined by the following flux relationship described by Loeb et al. [26] for FO mode:

$$K_D = \left(\frac{1}{J_w}\right)\ln\frac{B + A\pi_{D,b}}{B + J_w + A\pi_{F,m}} \tag{10}$$

Here B refers to the salt permeability coefficient of the membrane active layer that can be determined from rejection experiments in RO mode [22]:

$$B = \frac{A(1-R_s)(\Delta P - \Delta\pi)}{R_s} \tag{11}$$

where R_s is the salt rejection of the membrane, ΔP the applied pressure during RO rejection test and $\Delta\pi$ is the osmotic pressure difference across the membrane.

Therefore, the water flux shown by Eq. (2) has to be modified to take into account the concentrative ECP and dilutive ICP phenomenon and the modified equation of the water flux in the FO process is given as follows [27]:

$$J_w = A\sigma[\pi_{D,i} - \pi_{F,m}] \quad (12)$$

Combining Eqs. (3) and (8) with (12), the following shows the modified water flux equation in the FO process.

$$J_w = \frac{1}{K_D}\ln\left[\frac{A\pi_{D,b}+B}{A\pi_{F,b}\exp(J_w/k_F)+J_w+B}\right] \quad (13)$$

2.3. Numerical modelling of the FO membrane module and solution properties

2.3.1. Numerical modelling of FO module

The established models for the FO process discussed in the earlier section were used to simulate the conditions in a plate-and-frame FO modules. The plate-and-frame FO membrane module was assumed to be made up of 10 connected leaves arranged to flow in series and each with a channel dimension of 1.44 m length, 1.0 m width and 1.14 mm spacer thickness on both sides of the membrane. Both cross flow directions were adopted: co-current crossflow (DS and FS flow in the same direction) and counter-current crossflow (DS and FS flow in opposite direction on each side of the membrane). Simulations were performed by assuming a plug-flow regime. For the purpose of mathematical calculation, the length x of the channel was divided into 10 different sections, each of length Δx and unit width, giving an area of Δx as illustrated in Fig. 1. The channel height in the membrane module is usually small and the mixing is enhanced by spacers; hence, the velocity variation in the y-direction has been assumed to be negligible.

During the operation of the FO process, the solute concentrations change along the length of the channel as shown in Fig. 1. The concentration profile of the DS is expected to be decreasing along its channel flow direction while the FS is expected to be increasing along its channel flow. Under the counter-current crossflow mode, the concentration profile of the FS will increase along the negative x-direction, as the flow is in opposite direction of the DS flow. The change in the concentration profile along the channel length also alters the other properties of the fluid that are

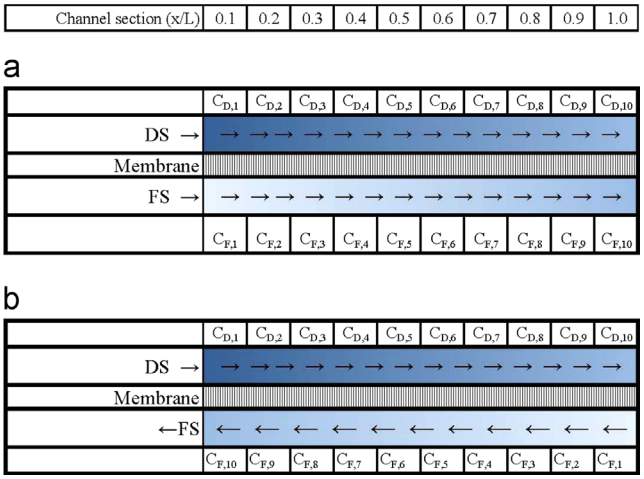

Fig. 1. Mathematical modelling for simulation of conditions in the membrane channel during the FO process under (a) co-current crossflow direction and (b) counter-current crossflow direction. C_D and C_F refer to the bulk concentrations of DS and FS, respectively, while the arrows indicate the direction of the crossflow.

Table 1
Essential parameters used during mathematical modelling for simulation in the FO membrane module.

Parameters	Values
Membrane parameters	
Membrane material	CTA
Pure water permeability coefficient, A (L m^{-2} h^{-1} bar^{-1})	1.020
Salt (NaCl) permeability coefficient, B (L m^{-2} h^{-1})	0.464
Module dimensions	
Number of leaves in the assembly	10
Length of each leaf (m)	1.44
Channel width (m)	1.00
Channel height (mm)	1.44
Draw solution	NaCl
Feed solution	NaCl
Solution temperature (both DS and FS)	25 °C

concentration dependent, such as osmotic pressure, diffusion coefficient, density, viscosity and hence the mass transfer coefficient of the FS. All these effects have been taken into consideration when simulating the osmotic process along the length of the channel in an FO membrane module. The variations of these parameters with solute concentrations are discussed separately in Section 2.3.2.

The mathematical models were solved iteratively and numerically because the equations in the model are implicit and highly nonlinear when ICP and ECP are taken into considerations [28]. The change in the conditions along the length of the channel (x-direction) such as flow rates, water flux, and solute concentrations were all taken into account for modelling. The mass transfer coefficient also changes with the change in the flow conditions and the FS properties along the channel [29] and this effect was accounted for in the simulation. Key parameters used in the simulation are provided in Table 1.

The numerical calculation for flow simulation along the membrane channel was quite straightforward for the co-current crossflow mode as the bulk concentration differences at the inlet of the DS and FS are known. However, for counter-current crossflow mode, calculation was not straightforward since one of the concentrations of the solution at each end of the module is unknown. In this case, the calculation was performed by first assuming that the FS was already flowing fully in the channel and the DS was then introduced. Calculations for the change in bulk concentrations and so the water flux along the channel length (x-direction) were performed by applying a mass balance equation and the modified flux equations presented in Eq. (13) for each section of the module, one by one before moving to the next section.

2.3.2. Thermodynamic properties of the feed and draw solutions (osmotic pressure, solution density, solution viscosity and solute diffusion coefficient)

The variation of thermodynamic properties (osmotic pressure, density, viscosity and diffusion coefficient) at various concentrations of the DS and FS were simulated using OLI Stream Analyser 3.2 (OLI Systems Inc., Morris Plains, NJ).

The osmotic pressure (π in atm) of NaCl as a function of molar concentration (C) is given by the following equation, which was obtained by fitting the simulated data in Fig. 2(a):

$$\pi = 3.805C^2 + 42.527C + 0.434 \quad (14)$$

Fig. 2(a) shows the non-linear variation of osmotic pressure with NaCl concentration and this explains why van't Hoff equation (1) is not useful for high concentration solutes.

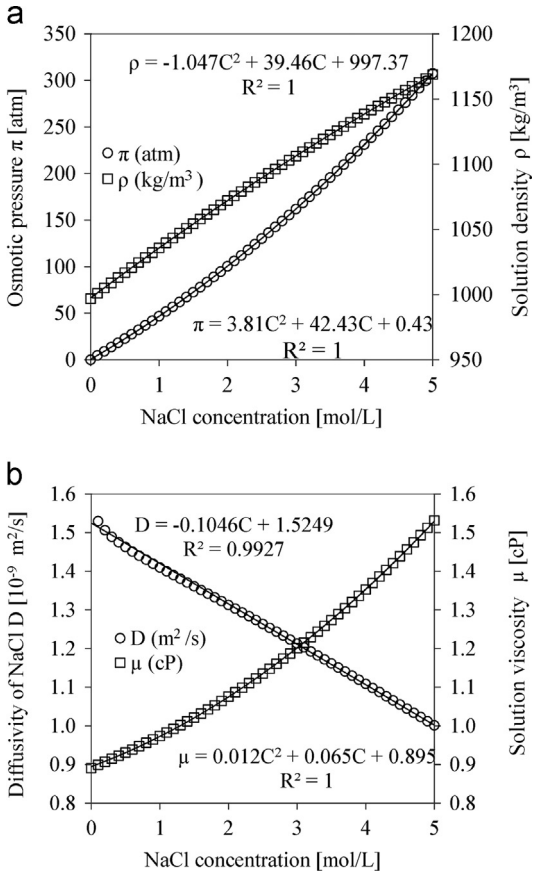

Fig. 2. Variation of the modelling parameters: (a) osmotic pressure and the density of the NaCl solutions and (b) viscosity and diffusion coefficient of NaCl solutions. These parameters were generated using OLI Stream Analyser 3.2.

Solution density (ρ) is important when calculating the kinematic viscosity (ν) of the solution. The relationship between solution density and NaCl concentration is obtained from fitting the simulated data shown in Fig. 2(a):

$$\rho = -1.047C^2 + 39.462C + 997.370 \quad (15)$$

The viscosity of the solution is an important parameter that affects the mass transfer in FO. The relationship between viscosity (μ) and NaCl concentration is given by the following equation obtained from fitting the simulated data presented in Fig. 2(b):

$$\mu = 0.012C^2 + 0.065C + 0.895 \quad (16)$$

Kinematic viscosity is then calculated using the following relationship from the data obtained from Eqs. (15) and (16):

$$\nu = \frac{\pi}{\rho} \quad (17)$$

The diffusion coefficient (D) of solutes plays an important role in the mass transfer of feed and solute resistivity of the DS that accounts for the impact of dilutive ICP [27,30–33] as evident from Eqs. (4) and (9). The average diffusion coefficient (D_{avg}) of NaCl was calculated using the individual diffusion coefficients of Na^+ and Cl^- ions using the following equations [34–36]:

$$D_{avg} = \frac{|Z_1| + |Z_2|}{(|Z_2|/D_1) + (|Z_1|/D_2)} \quad (18)$$

where Z_i is the cation/anion charge of the ionic species and D_i is the individual diffusion coefficient of the cation/anion species in water. The concentration dependence of D is provided by the following relationship obtained by fitting the simulated data shown in Fig. 2(b):

$$D = (-1.025 \times 10^{-10})C + 1.518 \times 10^{-9} \quad (19)$$

3. Experimental

Experiments for validating the FO water flux models described by Eq. (13) were conducted using a flat-sheet cellulose triacetate (CTA) membrane (Hydration Technologies Innovations, Albany, OR) in a bench-scale FO unit, containing an acrylic membrane cell with channel dimensions of 7.7 cm × 2.6 cm × 0.3 cm (on both sides of the membrane). The pure water permeability coefficient (A) of the CTA membrane was tested in RO mode at different applied pressures ranging 5–15 bar. The RO cell had similar dimensions to that of the FO cell and the average value of A was found to be 1.015 L m^{-2} h^{-1} bar^{-1}. This membrane is similar to those used in our previous studies [4,19]. The other characteristics of this CTA FO membrane are widely reported elsewhere [6,32,37]. The schematic layout of the bench-scale FO test unit is provided in our earlier publications [4,19,38].

All lab scale experiments were operated in FO mode (active layer facing FS) and in counter-current flow directions, at a cross-flow rate of 8.5 cm/s (400 ml/min), and at a temperature of 25 °C for a duration of at least 4 h for each experiment. The initial volume of DS and FS was 2 l in all cases and the experiments were conducted in a batch process, meaning the solutions were recycled back to their respective tanks after passing through the membrane. The water flux was chosen from the initial stage of the run (usually within the first 30 min of starting the FO process) since it continued to decrease with time due to continuous dilution of the DS and continuous concentration of FS tanks. The water flux was recorded by measuring the change in DS volume using a digital mass scale connected to PC for online data recording.

4. Results and discussion

4.1. Experimental validation of the water flux model and osmotic equilibrium in the FO process

Fig. 3 shows the variation of experimental water flux (square symbols) with the DS concentration obtained from the bench-scale FO unit described before. The feed water consisted of 35 g/L NaCl (seawater TDS) and NaCl solutions at various concentrations

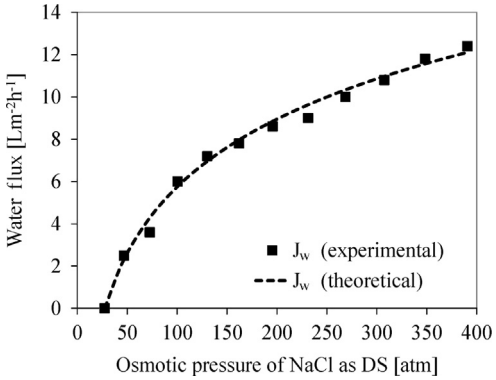

Fig. 3. Comparison between the experimental water flux and the predicted water flux using Eq. (13) in FO at various NaCl DS concentrations (represented by osmotic pressure of NaCl DS). Predictions were made by accounting for the variations in the thermodynamic properties of the DS at different concentration, with 35 g/L NaCl as feed water (seawater quality) using the FO cell dimensions described in Section 3. Experiments were conducted under counter-current crossflow condition at 400 ml/min for both DS and FS. Solution temperatures were kept at 25 °C.

were used as DS. The predicted water flux using Eq. (13) is shown by a dashed line in the same plot. The experimental and the predicted water fluxes match very closely, validating the water flux models for the FO process. Based on these successful results, this model will be used in the next sections to simulate the water flux in the membrane module.

It is natural to assume that osmotic equilibrium is a point at which the osmotic pressure of the solutions on each side of the membrane becomes equal. At this point, the net transfer of water across the membrane is zero. If similar solutes are present on both sides of the membrane, the equilibrium means that they have the same or equal concentrations. Irrespective of the types of draw solutes present on each side of the membrane, equilibrium will occur only when the osmotic pressure of the two solutions are equal at the membrane surface.

Experiments were conducted to observe whether equilibrium in the FO process occurs when the bulk osmotic pressures of the DS and FS become equal. First, a series of experiments were conducted using NaCl as both draw and feed solute and at equal bulk concentrations. In the second set of experiments, the FS concentration was maintained the same while the DS concentrations were varied. The DS concentrations varied only slightly around the FS concentration to mimic the diluted DS reaching the point of osmotic equilibrium. This also allows the observation of the osmotic process at a microscopic level during the osmotic equilibrium.

Fig. 4 shows the water flux in the FO process under the various DS and FS concentrations. When the bulk concentrations of the DS and FS are equal, the net water flux across the membrane is zero or almost zero (Fig. 4(a)). This was true for all the osmotic equilibrium experiments conducted at different bulk concentrations. This observation therefore confirms the osmotic equilibrium in the FO membrane module would occur at equal bulk concentrations or at equal bulk osmotic pressures. In the next set of experiments, the FS was fixed at 0.6 M NaCl (seawater quality) and the DS concentrations (NaCl) were varied around this FS concentration. As expected, the water flux is positive when the DS bulk concentration is higher than the feed bulk concentration and negative when the DS bulk concentration is lower than FS bulk concentration. However, joining the plots of water flux for the positive and negative flux cases provides an *x*-intercept of 0.6 M NaCl at which point the water flux is zero. The 0.6 M NaCl is the same as the FS concentration used for this experiment. The results further confirm that osmotic equilibrium in the FO process is reached when the bulk osmotic pressures of the DS and FS are equal. This observation is not surprising since the water flux at osmotic equilibrium is zero and hence ECP and ICP are non-existent.

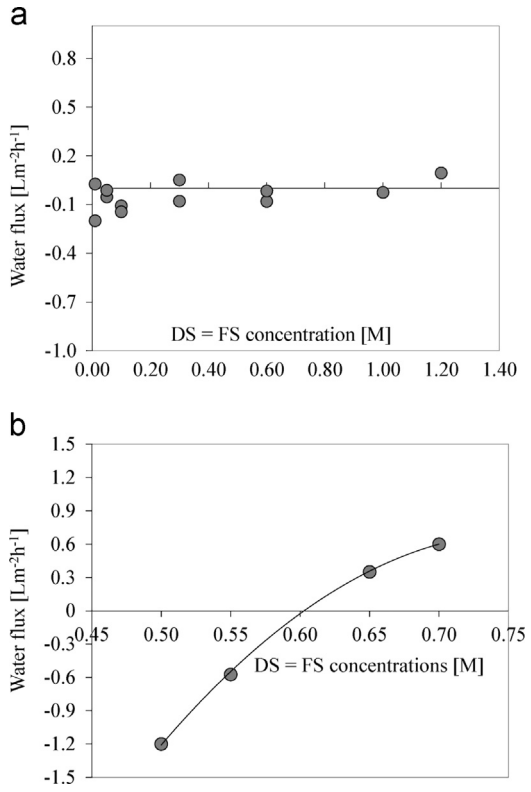

Fig. 4. Experimental water flux in the FO process when (a) NaCl DS and FS bulk concentrations are equal (at the point of osmotic equilibrium) and (b) 0.6 M NaCl as FS and at different DS concentrations. Experiments were conducted under counter-current crossflow conditions at 400 ml/min for both DS and FS. Solution temperatures were kept at 25 °C.

The plot of water flux versus DS concentration presented in Fig. 4(b) also confirms reports in many earlier publications that the water flux varies logarithmically with the bulk concentration when the DS concentration is higher than the FS [4,37–41]. The other observation from Fig. 4(b) is the higher negative water flux compared to the positive water flux, although they arose with similar bulk concentration difference between the two solutions. This is because the water flux in PRO mode of operation (DS facing the active layer) is higher than in FO mode of operation since the concentrative ICP in PRO is less severe than the dilutive ICP in FO mode [25,32,42,43]. When the DS concentration is made lower than the FS, the water flux reverses and the FO operates in PRO mode.

4.2. *Influence of crossflow direction on the point of osmotic equilibrium*

This section demonstrates the influence of crossflow directions on the point of osmotic equilibrium and its implications in the FO process. The variations of process parameters, such as water flux, DS and FS concentrations and feed recovery rates have been simulated along the length of the channel in an FO membrane module. The simulation was first performed by assuming a module of membrane area (144 m^2) using 100 and 35 g/L of NaCl as DS and FS, respectively, and the simulation results are presented in Fig. 5.

Two different water fluxes have been characterised to study its variation along the length of the channel in a membrane module. The first refers to the local water flux (represented by $J_{w,x}$ in Fig. 5(a)) at each section along the channel length assuming a plug flow-regime, while the second flux refers to the cumulative average water flux ($J_{w,a}$) along the channel in the membrane module. The water flux that comes out at the end of the module is the cumulative average water flux for the whole channel length and membrane area of the FO membrane module and is termed as the module average water flux. Fig. 5(a) shows the variation of water flux and the feed recovery rates along the channel length of a plate-and-frame FO membrane module.

Both water fluxes (local and the average water fluxes) decrease along the channel length of the membrane module irrespective of the crossflow directions. The decrease in the local water flux along the channel is attributed to the change in the driving force (or concentration difference) associated with the change in the DS and FS concentrations along the channel length, as shown in Fig. 5(b) by dotted lines. This decrease in local water flux also, in turn, decreases the average water flux along the channel length. The decrease in water flux is more rapid for an FO module operated in co-current crossflow mode, while under counter-current crossflow mode, the water flux decrease is more gradual. The very high water flux observed at the initial sections of the channel for co-current crossflow mode is due to the existence of a very high concentration difference at the start of the channel as shown in

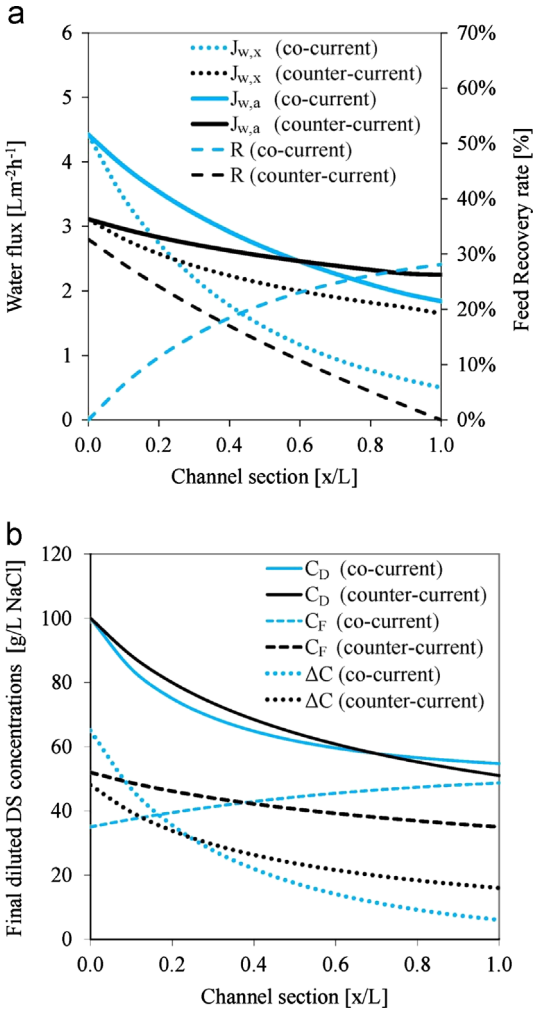

Fig. 5. Variation of (a) local water flux and local feed recovery rates and (b) local bulk DS/FS concentrations and concentration differences along the length of the channel (shown by dimensionless channel section x/L) in a membrane module under co-current and counter-current crossflow mode. $J_{w,x}$ represents local water flux for each channel sectional area and $J_{w,a}$ represents cumulative average water flux at each channel section point. Simulation conditions include total membrane area = 144 m^2, initial FS flow rate = 1.00 m^3/h, initial DS flow rate = 0.34 m^3/h, initial DS concentration = 100 g/L NaCl, initial FS concentration = 35 g/L, and solution temperature 25 °C.

Fig. 5(b). Co-current crossflow in the FO process is therefore likely to result in higher scaling/fouling at the entrance of the membrane module due to the high water flux and the high local feed recovery rate generated by the large driving force. Recent studies have indicated that operating the FO process above the critical flux could accelerate membrane scaling and membrane fouling due to high feed recovery rates [44]. The local water flux and the average water flux are similar at the beginning of the channel, but the local water flux decreases significantly at the end sections of the channel. The final average water flux that comes out of the channel is the module average water flux and this depends on the length of the channel or the total membrane area of the module.

The water flux in fact decreases non-linearly along the channel length for both co-current and counter-current modes, although the degree of non-linearity is more evident for co-current mode. This non-linearity in the average water flux can be explained due to dilutive ICP and concentrative ECP effects at the earlier sections of the channel. Since the concentration differences are higher within the initial sections of the module channel (Fig. 5(b)), it generates higher water fluxes that in turn exacerbate the CP effects. This non-linearity of the water flux with the DS concentrations has already been reported in many earlier studies [4,11,25,37,38,42] and may also be observed in Fig. 4(b). The water flux, however, becomes linear in the latter sections of the channel as the concentration difference gradually decreases. The water flux simulation in Fig. 5(a) shows that, under the counter current mode of operation, the module average water flux will be higher and consequently a higher dilution factor can be achieved for the final diluted DS.

Fig. 5(b) shows the variation of bulk DS and FS concentrations along the length of the channel. The DS concentration decreases along the DS channel because of the dilution by the incoming water flux from the feed side, while on the contrary, the FS concentration increases along its channel. The increase in feed concentration along the length of the channel is the same irrespective of crossflow modes (Fig. 5(a)), except that for counter-current mode, the increase in FS concentration happens in opposite direction, towards the left side of the plot (refer Fig. 1 for crossflow directions). The bulk DS concentration sharply drops at the initial sections of the module for co-current crossflow mode while for counter-current mode, the decrease in the DS concentration is more or less gradual (Fig. 5(a)). The sharp drop in the DS concentration at the entry sections is because of the higher water flux generated due to higher concentration difference for co-current mode than for the counter-current mode. However, further downstream of the module, the DS concentration gradually decreases as the water flux continues to decrease along the length of the channel.

The bulk DS concentration at the channel outlet ($x/L = 1.0$) determines the extent of the dilution of the DS in the membrane module. Fig. 5(b) shows the variations of DS and FS bulk concentrations along their respective channel lengths, and it is worthwhile to note the difference between the co-current and counter-current crossflow directions. In the co-current crossflow mode, DS and FS travel in the same direction along the channel length. The DS becomes more diluted while the FS becomes more concentrated as they travel along the channel length. This change in the DS and FS concentrations leads to a decrease in the concentration difference or driving force along the channel length, and hence decrease in the local water flux. If enough volume of water crosses the membrane from FS to the DS side (depends on the membrane area), osmotic equilibrium could be reached at the end of the channel where the bulk concentrations of DS and FS would become equal and the local flux would become zero. We can therefore conclude that, under co-current crossflow mode in FO process, osmotic equilibrium will be reached when the final concentration of the diluted DS becomes equal to the final concentration of the feed concentrate. This implies that the maximum dilution of the DS that can be achieved is equivalent to the concentration of the feed concentrate, which depends on the feed recovery rate.

In the counter-current crossflow mode of FO operation, the DS and the FS travel along the channel length, but in the opposite directions to each other (Fig. 1). Although the DS becomes diluted along the channel, it travels along the direction in which the FS concentration is lower than the feed concentrate, with maximum feed concentration being at the inlet point of the DS. The consequence of this is that the decrease in the concentration difference along the length of the channel is not as rapid as observed under co-current mode as shown in Fig. 5(b). If a sufficient volume of water crosses the membrane, the osmotic equilibrium will be reached when the diluted bulk DS concentration is equal to the bulk concentration of the feed solution at the FS inlet (or DS outlet). This implies that under the counter-current crossflow mode of FO operation, the maximum dilution of DS that can be achieved is equivalent to the initial concentration of the FS, and hence does not depend on the feed recovery rate.

Based on the point of osmotic equilibrium, the simulation results indicate that the extent of dilution of the DS in the FO process will be higher if it is operated in the counter-current crossflow mode rather than the co-current mode. Although the concentration differences within the initial sections of the channel are higher for co-current mode, within most of the latter sections, the concentration difference remains higher for counter-current mode, resulting in higher module average water flux. Besides, the counter-current mode of FO operation also offers other advantages such as gradual decrease of water flux in the module channel and hence lower fouling/scaling potential. Loeb and Bloch [45] also noted that operating the FO process in a counter-current crossflow direction could provide a constant driving force along the membrane module which could make the process more efficient, a process similar to the operation of heat exchangers [45].

Feed recovery rate is directly influenced by the total membrane area and hence the variations of module average water flux. Feed recovery and final concentration of the diluted DS are plotted against total module membrane area in Fig. 6. The simulated results show that when the FO process is operated using a module with larger membrane area, the influence of crossflow mode (co-current or counter-current) becomes more significant. The water flux and feed recovery rates (Fig. 6(a)) are not only higher but the final dilution factor of the DS is much higher and hence a much lower final DS concentration (Fig. 6(b)) for FO process operated in the counter-current crossflow mode. It is clear from the simulation that the crossflow direction could play a significant role when a larger membrane area is used to achieve a higher feed recovery rate in the FO process. However, when a larger membrane area is used in the membrane module, the increased feed recovery rate will also reduce the module average water flux as indicated in Fig. 6(a). This is similar to pressure driven membrane processes in which the feed recovery rate increases when larger membrane modules are used [46–48]. Hence, for a known DS and FS concentration, the total membrane area may be determined based on the target final concentration of the diluted DS, because this final DS concentration has a significant bearing on the post-treatment process.

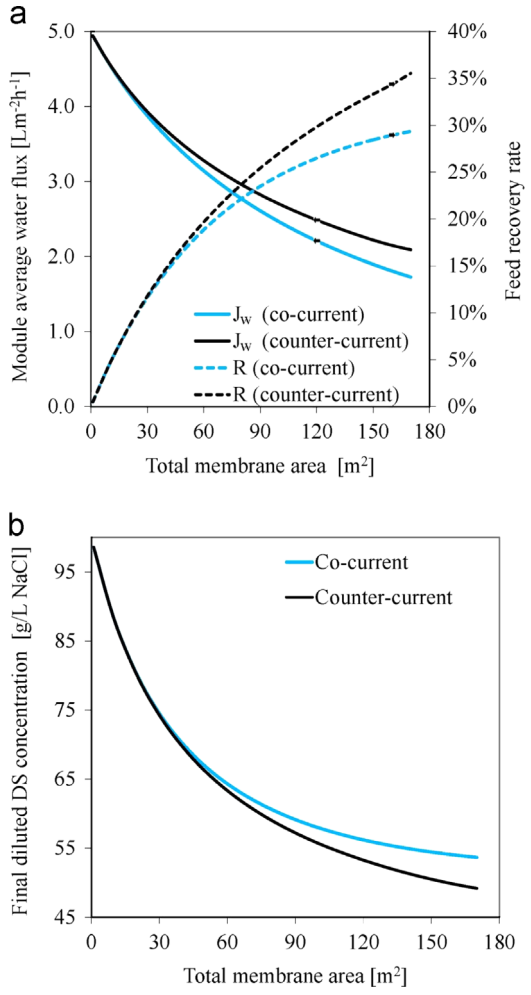

Fig. 6. Variation with membrane area of the FO membrane module of (a) the module average water flux and feed recovery rates and (b) the final concentration of the diluted DS under co-current and counter-current crossflow modes. Simulation conditions include initial FS flow rate = 1.00 m^3/h, initial DS flow rate = 0.34 m^3/h, initial DS concentration = 100 g/L NaCl, initial FS concentration = 35 g/L, and solution temperature 25 °C.

4.3. Influence of initial solution concentrations on osmotic equilibrium

4.3.1. Influence of initial draw solution concentration

In earlier studies, it was observed that water flux increased with an increase in DS concentration, although this increase was generally logarithmic in which case the increase in water flux becomes non-linear when higher DS concentrations are used [4,11,25,37,38,40–42]. As discussed earlier, this non-linearity in water flux is caused by the enhanced CP effects at higher water flux generated due to higher concentration differences. The influence of the initial DS concentrations on the final concentrations of the diluted DS, the module average water flux and the recovery rates are shown in Fig. 6.

Fig. 7(a) shows the variation of the module average water flux and feed recovery rates at various initial DS concentrations. The average water flux increases when higher initial DS concentrations are used and this increase is non-linear. This non-linearity in water flux was evident for both crossflow modes of the FO process. However, it must be noted that the average water flux for the counter-current crossflow mode is consistently higher than for the co-current mode, indicating the advantage of the counter-current mode over the co-current mode of operation. This higher average water flux under the counter-current mode is a result of the higher and consistent concentration differences that exist along the membrane channel when operated in counter-current mode (as discussed in the earlier section). The feed recovery in Fig. 7(a) also increased with the initial DS concentration and showed a similar non-linear trend to the water flux, which is expected given the direct correlation between the water flux and feed recovery rate.

Fig. 7(b) shows the simulation results of the variation of the final diluted DS concentrations when different initial DS concentrations are used in the FO process. For a fixed membrane area, when higher initial DS concentrations are used, the concentration of the final diluted DS will also be correspondingly higher, irrespective of the crossflow directions used. Even though the local water flux generated increases at higher DS concentration, the local water flux and membrane area are not adequate for the osmotic process to continue within the given length of the module and therefore the diluted DS exits the module outlet without reaching the point of osmotic equilibrium. This is the reason why the concentration of the final diluted DS remains high when the initial DS concentration used is high. The other observation from Fig. 7(b) is the difference in the final concentration of the diluted DS between co-current and counter-current crossflow modes. The FO process operated under the counter-current mode will achieve significantly lower final diluted DS concentrations than under co-current crossflow mode, which supports our earlier findings on the advantages of counter-current crossflow mode.

What, therefore, is the ideal initial DS concentration for the FO module during the FO desalination process for a fixed membrane

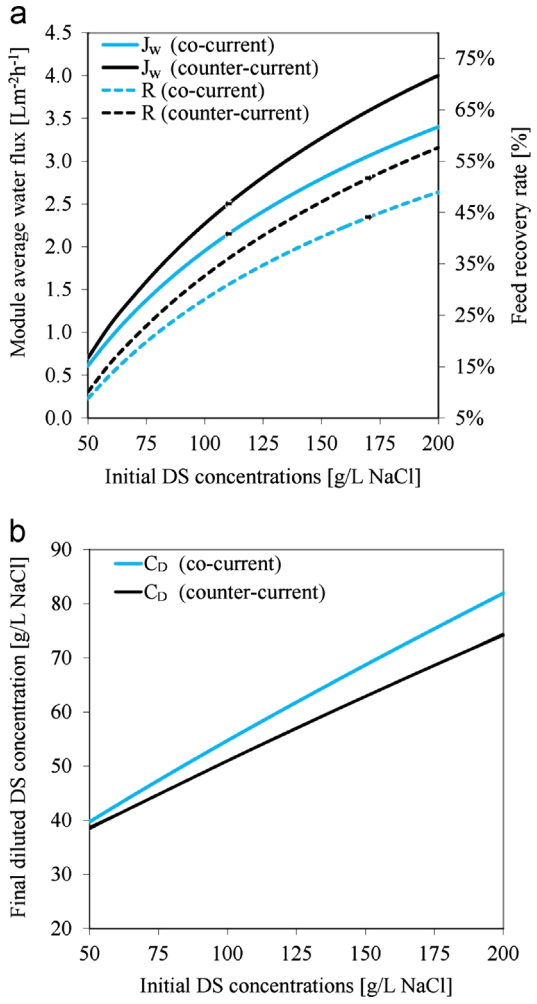

Fig. 7. Variation of (a) the module average water flux and feed recovery rates and (b) the final concentration of the diluted DS under co-current and counter-current crossflow mode at different initial DS concentrations. Simulation conditions include total membrane area = 144 m^2, initial FS flow rate = 1.00 m^3/h, initial DS flow rate = 0.34 m^3/h, initial FS concentration = 35 g/L, solution temperature 25 °C.

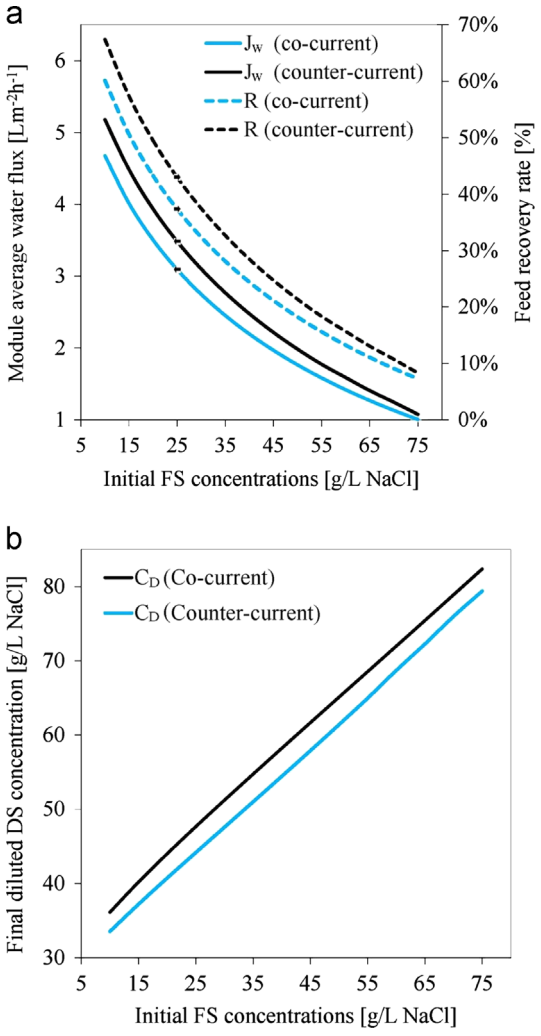

Fig. 8. Variation of (a) the module average water flux and feed recovery rates and (b) the final concentration of the diluted DS under co-current and counter-current crossflow modes at different initial FS concentrations. Simulation conditions include total membrane area = 144 m^2, initial FS flow rate = 1.00 m^3/h, initial DS flow rate = 0.34 m^3/h, initial DS concentration = 100 g/L, and solution temperature 25 °C.

area or number of modules? A close inspection of Fig. 7(a) reveals that when the initial DS concentration is 50 g/L, the final diluted DS concentration reaches a value of about 38.5 g/L, a value very close to the initial FS concentration of 35 g/L simulated for a membrane area of 144 m^2 in this study. This shows that although higher module average water flux could be achieved by using DS concentration higher than 50 g/L, the final diluted DS will also be proportionately higher. A larger membrane area may therefore be required to achieve further dilution of the final DS.

For practical operations, one needs to choose a suitable initial concentration level for the DS [49]. For a fixed membrane area, this initial DS concentration must also be guided by the target concentration level of the final diluted DS that consequently affects the quality of the water for direct use or the amount of energy required for any post-treatment process. If too high a concentration is used, it may not only reduce the process efficiency [49], but also increase the energy required for pumping due to the increased fluid viscosity of the DS.

4.3.2. *Influence of initial feed solution concentration*

Besides the initial DS concentration, the initial feed TDS or FS concentration may also have a significant influence on the variation of performance parameters in the FO process. Fig. 8 shows the variation of the module average water flux, the final diluted DS concentration and the feed recovery rate with the initial feed concentrations. The module water flux and the feed recovery rate decrease with an increase in feed TDS due to reduced driving force across the membrane as shown in Fig. 8(a). This decrease in average water flux is non-linear with the feed TDS because of the difference in the degree of concentrative ECP occurring on the active membrane surface exhibited by the differences in the net driving force and the water flux. The ECP modulus decreases with the decrease in water flux at higher TDS feed as evident from Eq. (3). Similar to earlier results, operating the FO process under counter-current cross-flow can achieve higher average water flux and feed recovery rates than under the co-current crossflow mode as shown in Fig. 8(a).

From our earlier observation in Fig. 5(b), the initial feed concentration determines the final osmotic equilibrium, especially for an FO process operated under counter-current crossflow mode. Fig. 8(b) shows the final concentration of the diluted DS when different initial feed TDS concentrations are used in the FO process. It is clear from the simulation results that the final diluted DS concentration will increase when a feed with higher TDS is used. The maximum dilution of the final DS could occur only under the counter-current mode, and the lowest DS concentration

that can be achieved under this condition is equivalent to the initial feed TDS or FS concentration.

From the above discussion, we can conclude that the FO process simply converts the saline feed water to diluted DS of equivalent bulk concentration, and that without external intervention, the final DS would never exhibit equivalent concentration lower than the FS. This is perhaps one of the major limitations of the FO process, especially if the final diluted DS requires further post-treatment for the separation of the draw solutes and the pure water. The simulation results have important implications for the application of the FO process for treatment of very high TDS feed waters, such as RO brine and processed water generated during the shale gas extraction [50]. The final concentration of the diluted DS from the treatment of such high TDS feed waters will still be proportionately high and further treatment of this diluted DS would be a major challenge, especially when separation of draw solutes from the water is essential.

4.4. *Influence of cross-flow rates on module average water flux, feed recovery rate and final concentration of the diluted DS*

4.4.1. *Influence of draw solution flow rate*

The influence of DS flow rate on the module average water flux, final diluted DS concentration and the feed recovery rate is simulated and plotted in Fig. 9. The increase in flow rate enhances the crossflow velocity rate or crossflow shear, and hence increases the mass transfer coefficient and the water flux. In addition, the higher flow rate also means a higher volume of the solution within the channel space that could have a significant impact on the dilution of the DS or the bulk concentration of the FS. This, in turn, affects the concentration difference on which the water flux and the final diluted DS concentration depend.

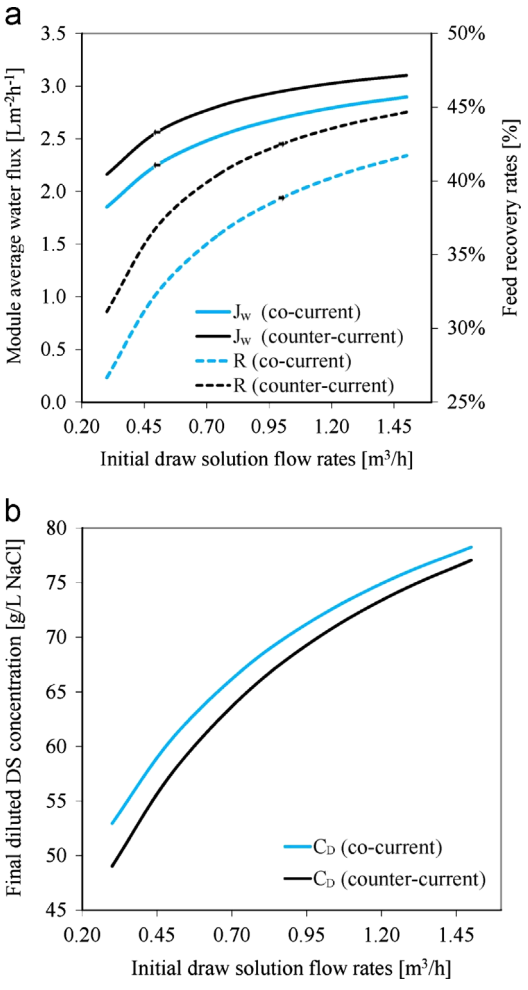

Fig. 9. Variation of (a) the module average water flux and feed recovery rates and (b) the final concentration of the diluted DS under co-current and counter-current crossflow mode at different initial DS flow rates. Simulation conditions include total membrane area = 144 m^2, initial FS flow rate = 1.00 m^3/h, initial DS concentration = 100 g/L, initial FS concentration = 35 g/L, solution temperature 25 °C.

Fig. 9 shows the simulation results of the influence of DS flow rate on the module average water flux, feed recovery rate and the final diluted DS concentration. The average water flux increases with the increase in the DS flow rate, but the increase is observed to be non-linear as shown in Fig. 9(a). The increase is more pronounced at the lower flow rate range than at the higher flow rate range. The increase in the water flux at higher flow rate can be attributed to the difference in DS dilution within the module channel at different flow rates. When the DS flow rate is increased, the volume and the mass of the draw solutes present within the channel increase proportionately, which helps to maintain higher concentration differences within the module channel. Although the initial water flux at the inlet region of the FO membrane module is expected to be similar, irrespective of the crossflow rate, as there exists a similar concentration difference as the DS travels along the channel in the module, the extent of dilution of the DS in the channel is lower when a higher DS flow rate is used. In other words, the incoming water flux from the feed does not dilute the DS as much as it would at a low flow rate. Hence, the bulk DS concentration gradient along the channel remains higher when higher DS flow rates are used. However, the trade-off for using a higher DS flow rate is a higher concentration of the final diluted DS as shown in Fig. 9(b). Similar results were obtained for the FO process simulated for co-current and counter-current crossflow modes of operation.

These results are in contrast to lab-scale results in which the water flux is not influenced significantly by the crossflow rate of the DS, in particular when the DS is facing the support layer under FO mode of operation [51–54]. This may be true because the lab-scale experiments are usually conducted using a small membrane area and membrane channel length where the recovery rate is very small and hence the effect is not detectable.

It is important to note here that the crossflow shear velocity of the DS does not affect the water flux because the DS that contributes to net osmotic pressure difference lies inside the membrane support layer, which is not affected by the outside hydrodynamic conditions [37]. This is also the reason why the first term in Eq. (13) for the water flux does not include the mass transfer coefficient. The water flux is in fact influenced by the structure of the membrane support layer shown by the parameter K, the draw solute resistivity of the membrane support layer.

The results in Fig. 9(a) also indicate that the optimum initial DS flow rate is in between 0.5 and 0.7 m^3/h for the conditions used for simulation in this study. The results further show that determining the initial DS flow rate is important for obtaining optimal module average water flux and final concentration of the diluted DS. Usually, a lower DS flow rate is adequate for the FO process since the flow rate increases along the length of the module due to influx of water from the feed side.

However, it is important to note here that the increase in the DS flow rate could be limited by the membrane and module design. Since the DS is located on the support layer side of the asymmetric polymeric FO membranes, the increase in DS flow rates would lead to build up of hydraulic pressure in the channel that could undermine the structural integrity of the thin active layer without a support layer. It is for this reason that the newly developed FO membrane modules from HTI come with a strict flow rate condition and pressure ratings for DS facing the membrane support layer [55].

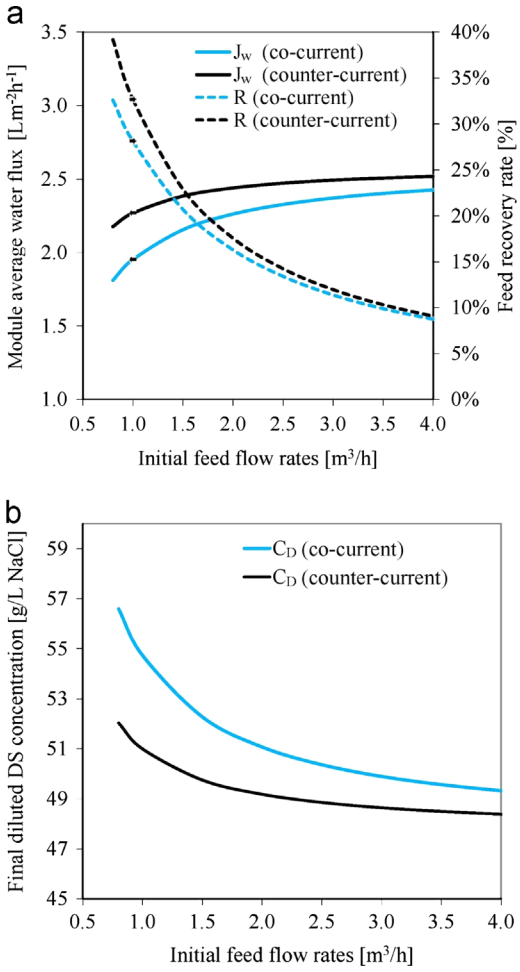

Fig. 10. Variation of (a) the module average water flux and feed recovery rates and (b) the final concentration of the diluted DS under co-current and counter-current crossflow mode at different initial FS flow rates. Simulation conditions include total membrane area = 144 m^2, initial DS flow rate = 0.34 m^3/h, initial DS concentration = 100 g/L, initial FS concentration = 35 g/L, solution temperature 25 °C.

4.4.2. *Influence of feed solution flow rate*

Fig. 10 shows the influence of feed flow rates on the module average water flux, feed recovery rate and the final diluted DS concentration. It is clear from Fig. 10(a) that the module average water flux and the feed recovery rate slightly increase with increase in the feed flow rate under both co-current and counter-current crossflow conditions. Besides higher average water flux, the other advantage of using higher FS crossflow rate is the lower concentration of the final diluted DS (Fig. 10(b)), although this would not be lower than the initial feed concentration if the osmotic process goes to the extent of osmotic equilibrium under the counter-current crossflow mode. The increase in the module average water flux in this case is mainly due to the increase in the crossflow velocity that reduces the concentrative ECP at the membrane active layer surface, and hence enhances the mass transfer coefficient of the feed side boundary layer (value of k_F in Eq. (4)), ultimately resulting in slightly improved water flux. However, Fig. 10(a) shows that operating FO at higher feed flow rates lowers the feed recovery rate. Lower feed recovery means that the bulk concentration gradient of the FS along the length of the channel in an FO module is lower, and hence can generate higher water flux due to higher concentration differences. In such a case, the concentration of the feed water at the module outlet would still be lower, requiring a second stage FO process to increase the feed recovery rate.

Similar to the earlier results with DS flow rates in Fig. 9, the influence of FS flow rates is more prominent at lower feed flow rates. At higher feed flow rate, the influence is not significant, irrespective of the crossflow direction, which suggests that operating the FO process at higher flow rates will not derive additional benefits, but rather increase the pumping energy. However, it is also worthwhile to note here that this increase in water flux with the feed flow rate is not as significant as that with the increase in the DS flow rate in Fig. 9. This is in contrast to lab-scale results in which the feed flow rate is reported to influence the water flux more than the DS flow rate, especially when the FO process is conducted in FO mode [53,54]. This is because in FO mode of operation, the DS within the membrane support layer is not affected by the hydrodynamic conditions occurring outside the support layer [37]. As discussed in the earlier section, the reason for not observing significant effects in lab-scale studies is the much smaller membrane area used, where the feed recovery is very small (less than 5%), and the effect is likely suppressed within experimental errors. In the earlier studies, Jung et al. [56] observed that the influence of feed flow rate on the water flux is not significant in the FO process. Even if a slight increase in water flux is observed, it significantly reduces the feed recovery rate when higher crossflow rates or higher feed flow rates are used [56].

In lab-scale experiments, similar flow rates are commonly used for most experiments and this develops similar flow conditions in the channel because of the small membrane area used. However, at a module level scale, maintaining similar flow rates for both DS and FS may not be practical as it could build pressure within the DS channel and undermine the integrity of the membrane active layer that is not supported [55].

4.5. *Implications of osmotic equilibrium for overall FO process performance*

From the above results, it is evident that in a large-scale FO process plant, the crossflow direction will have a significant influence on the point of osmotic equilibrium, and hence on the overall performance of the process, such as the module average water flux, the feed water recovery rate and the final concentration of the diluted DS. Since the performance parameters could ultimately have a bearing on the capital and operational costs, optimising the parameters that influence the performance is of paramount importance for any FO desalination processes. It will be an important decision for an FO plant designer to consider whether the module average water flux is more significant, or the extent of the final dilution of the DS in the FO process. This is because increasing the average water flux by increasing the initial DS concentration will result in higher concentration of the final diluted DS besides increasing the energy required for pumping.

The energy consumption for RO desalination increases with increasing recovery rate [17,57] and for practical purposes, RO desalination plants are usually operated around 50% recovery for sea water [58] and higher for brackish water with lower salinity content. However, for the FO process, a higher recovery rate can be achieved by simply operating in counter-current cross-flow mode and using a higher DS concentration that involves only a slight increase in energy consumption. FO has been acknowledged for its potential to achieve high recovery rate of the feed water [59,60], without requiring significant additional energy.

The other significant implication of the crossflow direction is the water extraction capacity of the draw solutes. We have shown in the earlier sections that the DS can extract water from the FS until the osmotic pressure of the DS reaches equilibrium with the osmotic pressure of the FS. The osmotic equilibrium, however, is attained at different concentration levels when the FO process is operated under different crossflow directions (counter-current or co-current).

Considering NaCl as both feed and draw solute, the water extraction capacity of the DS can be estimated. An NaCl DS can extract water from an NaCl FS as long as the concentration of the DS is higher than the FS. If the FS concentration is very high, say equivalent to the maximum solubility ($C_{D,max}$) of the NaCl, then the NaCl DS cannot extract any water from the FS as the DS concentration cannot be made higher than $C_{D,max}$. The total volume of water (V) a kilogram of NaCl as draw solute can extract from an NaCl feed of concentration ($C_{F,0}$) can be estimated using the following relationship derived from the mass balance calculations:

$$V = \frac{1000}{M_w}\left[\frac{1}{C_{F,0}} - \frac{1}{C_{D,max}}\right] \quad \text{[under counter – current crossflow mode]} \tag{20}$$

$$V = \frac{1000}{M_w}\left[\frac{(1-Rr)}{C_{F,0}} - \frac{1}{C_{D,max}}\right] \quad \text{[under co – current crossflow mode]} \tag{21}$$

where $C_{F,0}/(1-Rr)$ refers to the feed concentrate or brine with a feed recovery rate of Rr.

It is clear from Eqs. (20) and (21) that the water extraction capacity of the draw solute depends only on its properties, such as molecular weight (M_w), equivalent concentration of the draw solute with the feed and the maximum solubility concentration. In fact, the water extraction capacity varies inversely with the molecular weight and initial feed concentration ($C_{F,0}$). This shows that the water extraction capacity of the draw solute will not be affected by any other process parameters, including the membrane properties. The DS properties can affect other performance parameters, such as water flux, and water feed recovery rates.

$C_{F,0}$ in Eqs. (20) and (21) is valid only when both the DS and FS contain the same solutes. However, when different draw solutes are used, osmotic equilibrium does not mean equal concentration because the osmotic pressure of the DS depends on solute properties, such as a number of species formed in solution and their osmotic coefficient [61]. Therefore, when a solute used for the DS is different from the feed solute, Eq. (20) can be re-written as follows for counter-current mode of FO process:

$$V = \frac{1000}{M_w}\left[\frac{1}{C_{D,E}} - \frac{1}{C_{D,max}}\right] \tag{22}$$

where $C_{D,E}$ is the molar concentration of the DS that generates equal bulk osmotic pressure (osmotic equilibrium condition) with the osmotic pressure of a FS with a concentration $C_{F,0}$. Eq. (22) indicates that the volume of water a kilogram of solute can extract depends on the molecular weight of the draw solute used and the molar concentration of the DS at which it generates an equal osmotic pressure as the FS.

Eqs. (20)–(22) are slightly different from the calculations used earlier in our publications [4,5,18,19,53]. In this study, the equations have been modified to include the influence of the maximum solubility ($C_{D,max}$) of the draw solute, as it also limits the water extraction capacity of the draw solute

Based on Eqs. (20) and (21), the water extraction capacities of the draw solutes have been estimated and presented as a function of feed concentration in Fig. 11. The water extraction capacity of NaCl as DS has been plotted against the TDS of the feed water in Fig. 11(a) under counter-current and co-current modes of FO membrane module operation. The water extraction capacity of the DS decreases exponentially with an increase in the TDS of the feed water, irrespective of the crossflow conditions, because of the inverse relationship with the feed concentration observed in Eqs. (20) and (22). These results indicate that although water can be extracted by an FO process from a high TDS feed water such as RO brine, the volume of water extracted will be extremely limited because of the high osmotic pressure of the FS, and osmotic equilibrium will occur at a concentration equivalent to that of the RO concentrate. The final DS concentration will still remain significantly higher, and that could affect post-treatment processes if required. It is important to note the difference in water extraction capacity between the counter-current and co-current crossflow modes. Under the counter-current crossflow direction, the water extraction capacity is not affected by the feed recovery rate, while under the co-current crossflow condition, the water extraction capacity decreases with increasing the feed recovery rate, even using the same FS concentrations.

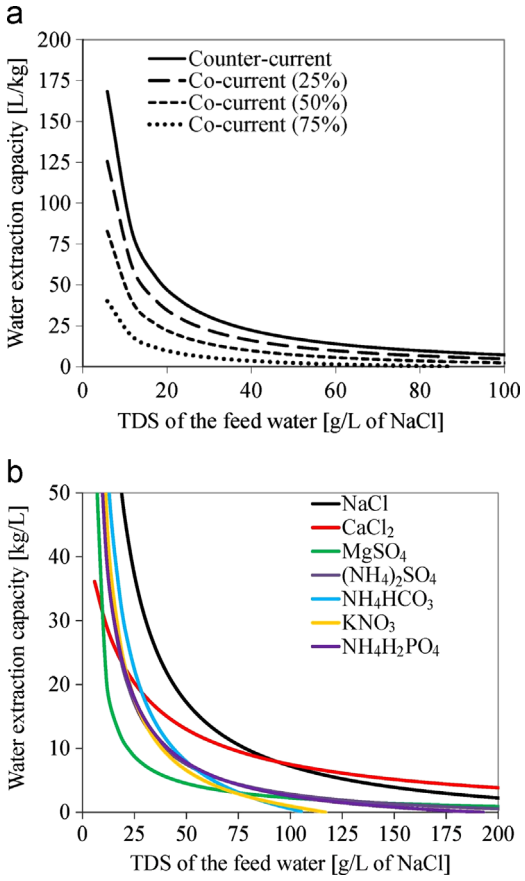

Fig. 11. Variation of water extraction capacities of the draw solutes by FO process at different feed TDS: (a) NaCl under different crossflow modes and (b) other selected draw solutes under counter-current crossflow mode.

Eq. (22) was used to estimate the water extraction capacities under counter-current cross-flow mode of selected other draw solutes that are widely reported in the literature. These are presented in Fig. 11(b). Similar to the results in Fig. 11(a) for NaCl, the water extraction capacities of all the other draw solutes decrease exponentially with an increase in feed TDS. NaCl, being the draw solute with lowest M_w, exhibits the highest water extraction capacity amongst all the selected solutes in this study. $CaCl_2$ is highly soluble and can generate one of the highest osmotic pressures. However, it is obvious from Fig. 11(b) that $CaCl_2$ as a draw solute will be more effective for high TDS feed water rather than low TDS feed water. NaCl could be effective for all ranges of feed TDS, indicating the prospects of RO concentrate or brine for use as DS for a wide range of FO applications. KNO_3 and NH_4HCO_3 are expected to be least effective when high TDS feed water is to be used for FO desalination. Although $MgSO_4$ has one of the least water extraction capacities at lower feed TDS, its capacity at higher feed TDS is comparable to other draw solutes such as $(NH_4)_2SO_4$ and $NH_4H_2PO_4$.

5. Conclusions

In this study, the significance of osmotic equilibrium in the FO process has been demonstrated by simulating the conditions in a plate-and-frame FO membrane module using established models under co-current and counter-current crossflow directions. The influence of various operational parameters, such as flow conditions within the membrane module channel, feed and draw solution properties and membrane area, were evaluated in terms of module average water flux, feed recovery rates and the final concentration of the diluted DS. The following conclusions can be drawn from this study:

- Crossflow direction plays a significant role in determining the point of osmotic equilibrium in the channel of an FO membrane module. An FO process operated in counter-current crossflow mode offers the following advantages over the co-current mode: (i) gradual decrease in the water flux along the length of the channel in an FO membrane module; (ii) higher average water flux of the membrane module; (iii) operation at higher feed recovery rate; (iv) higher dilution factor of the final DS and hence lower concentration of the final diluted DS from the FO membrane module; and (v) higher water extraction capacity of the draw solutes.
- Osmotic equilibrium is one of the most significant milestones in the FO process. It determines the extent of dilution of the DS, which ultimately affects the quality of the FO process product water. It must be noted that without external intervention, dilution of the DS beyond the point of osmotic equilibrium is impossible. The lowest concentration that the final diluted DS can achieve is equivalent to the initial feed concentration under counter-current crossflow mode and equivalent to the final feed concentration under co-current crossflow mode of FO operation.
- The point of osmotic equilibrium also influences the water extraction capacity of the draw solutes. A modified relationship has been proposed to estimate the water extraction capacity of the draw solutes based on osmotic equilibrium and mass balance. FO operated in counter-current mode could extract more water for a unit mass of draw solutes than under co-current mode.
- Optimisation of all process parameters is an important task for the efficient operation of the FO process. For example, although the use of a higher DS concentration could generate higher water flux, the final concentration of the diluted DS will remain higher for a fixed membrane area, indicating a trade-off that exists between the module average water flux and the final concentration of the diluted DS.

It is important that the limitations of this study be acknowledged. The simulation data for the plate-and-frame module could not be validated experimentally using actual membrane module. The water flux models used in this simulation are, however, widely used and accepted, and also validated in this study. The current simulation was conducted using similar solutes for both the DS and FS (NaCl). However, when the solutes for the DS and FS are different, a slight modification to the numerical analysis is necessary to account for the solute fluxes that can occur in both directions during the FO process.

Acknowledgements

This study was supported by the National Centre of Excellence in Desalination Australia (NCEDA), which is funded by the Australian Government through the Water for the Future initiative. This study was also partly supported by the World Class University Program funded by the Ministry of Education, Science and Technology through the National Research Foundation of Korea (R33-10046).

Nomenclature

A	pure water permeability coefficient ($L\,m^{-2}\,h^{-1}\,bar^{-1}$)
B	salt permeability coefficient ($m\,s^{-1}$)
C	solute concentration (mg/L or Moles or M)
D	diffusion coefficient ($m^2\,s^{-1}$)
d_h	hydraulic diameter (m)
J_w	water flux ($L\,m^{-2}\,h^{-1}$)
k	mass transfer coefficient ($m\,s^{-1}$)
K	resistance of solute diffusion within the membrane support layer (s/m)
L	length of the channel (m)
M_w	molecular weight (mol/g)
n	van't Hoff factor
P	applied hydraulic pressure (bar)
R	universal gas constant (0.0821 L atm $mol^{-1}\,K^{-1}$)
Re	Reynolds number
R_s	salt rejection (%)
Sc	Schmidt number
Sh	Sherwood number
T	absolute temperature (K)
π	osmotic pressure (atm or bar)
σ	reflection coefficient
ρ	density (kg/m^3)
μ	dynamic viscosity (cP)
υ	kinematic viscosity ($m^2\,s^{-1}$)
Z	cation/anion charge
V	volume of water extrated (L/kg)

References

[1] T.Y. Cath, J.E. drewes, C.D. Lundin, A Novel Hybrid Forward Osmosis Process for Drinking Water Augmentation Using Impaired Water and Saline Water Sources, WERC and Water Research Foundation, Denver, CO, 2009.
[2] T.-S. Chung, X. Li, R.C. Ong, Q. Ge, H. Wang, G. Han, Emerging forward osmosis (FO) technologies and challenges ahead for clean water and clean energy applications, Curr. Opin. Chem. Eng. 1 (2012) 246–257.
[3] L.A. Hoover, W.A. Phillip, A. Tiraferri, N.Y. Yip, M. Elimelech, Forward with osmosis: emerging applications for greater sustainability, Environ. Sci. Technol. 45 (2011) 9824–9830.
[4] S. Phuntsho, H.K. Shon, S.K. Hong, S.Y. Lee, S. Vigneswaran, A novel low energy fertilizer driven forward osmosis desalination for direct fertigation: evaluating the performance of fertilizer draw solutions, J. Membr. Sci. 375 (2011) 172–181.
[5] S. Phuntsho, H.K. Shon, S.K. Hong, S.Y. Lee, S. Vigneswaran, J. Kandasamy, Fertiliser drawn forward osmosis desalination: the concept, performance and limitations for fertigation, Rev. Environ. Sci. Biotechnol. 11 (2012) 147–168.
[6] T.Y. Cath, A.E. Childress, M. Elimelech, Forward osmosis: principles, applications, and recent developments: review, J. Membr. Sci. 281 (2006) 70–87.
[7] T.Y. Cath, D. Adams, A.E. Childress, Membrane contactor processes for wastewater reclamation in space: II. Combined direct osmosis, osmotic distillation, and membrane distillation for treatment of metabolic wastewater, J. Membr. Sci. 257 (2005) 111–119.
[8] R.W. Holloway, A.E. Childress, K.E. Dennett, T.Y. Cath, Forward osmosis for concentration of anaerobic digester centrate, Water Res. 41 (2007) 4005–4014.
[9] E.M. Garcia-Castello, J.R. McCutcheon, Dewatering press liquor derived from orange production by forward osmosis, J. Membr. Sci. 372 (2011) 97–101.
[10] A. Achilli, A.E. Childress, Pressure retarded osmosis: from the vision of Sidney Loeb to the first prototype installation – review, Desalination 261 (2010) 205–211.
[11] T.-S. Chung, S. Zhang, K.Y. Wang, J. Su, M.M. Ling, Forward osmosis processes: yesterday, today and tomorrow, Desalt 287 (2012) 78–81.

[12] Q. She, X. Jin, C.Y. Tang, Osmotic power production from salinity gradient resource by pressure retarded osmosis: Effects of operating conditions and reverse solute diffusion, J. Membr. Sci. 401–402 (2012) 262–273.
[13] N.Y. Yip, M. Elimelech, Thermodynamic and energy efficiency analysis of power generation from natural salinity gradients by pressure retarded osmosis, Environ. Sci. Technol. 46 (2012) 5230–5239.
[14] O.A. Bamaga, A. Yokochi, E.G. Beaudry, Application of forward osmosis in pretreatment of seawater for small reverse osmosis desalination units, Desalt. Water Treat. 5 (2009) 183–191.
[15] O.A. Bamaga, A. Yokochi, B. Zabara, A.S. Babaqi, Hybrid FO/RO desalination system: preliminary assessment of osmotic energy recovery and designs of new FO membrane module configurations, Desalination 268 (2011) 163–169.
[16] Y.-J. Choi, J.-S. Choi, H.-J. Oh, S. Lee, D.R. Yang, J.H. Kim, Toward a combined system of forward osmosis and reverse osmosis for seawater desalination, Desalination 247 (2009) 239–246.
[17] M. Elimelech, W.A. Phillip, The future of seawater desalination: energy, technology, and the environment, Science 333 (2011) 712–717.
[18] S. Phuntsho, S. Hong, M. Elimelech, H.K. Shon, Forward osmosis desalination of brackish groundwater: meeting water quality requirements for fertigation by integrating nanofiltration, J. Membr. Sci. 436 (2013) 1–15.
[19] S. Phuntsho, H.K. Shon, T. Majeed, I. El Salibya, S. Vigneswarana, J. Kandasamy, S. Hong, S. Leeb, Blended fertilisers as draw solutions for fertiliser drawn forward osmosis desalination, Environ. Sci. Technol. 46 (2012) 4567–4575.
[20] J.H. Van't Hoff, Die Rolle der osmotischen Druckes in der Analogie zwischen Lösungen und Gasen, Z. Phys. Chem. 1 (1887) 481–508.
[21] A. Yokozeki, Osmotic pressures studied using a simple equation-of-state and its applications, Appl. Energy 83 (2006) 15–41.
[22] K.L. Lee, R.W. Baker, H.K. Lonsdale, Membranes for power generation by pressure-retarded osmosis, J. Membr. Sci. 8 (1981) 141–171.
[23] S. Bhattacharjee, J.C. Chen, M. Elimelech, Coupled model of concentration polarization and pore transport in crossflow nanofiltration, AIChE J. 47 (2001) 2733–2745.
[24] M.C. Porter, Porter, C. Mark, Concentration polarization with membrane ultrafiltration, Ind. Eng. Chem. Prod. Res. Dev. 11 (1972) 234. (&).
[25] J.R. McCutcheon, M. Elimelech, Influence of concentrative and dilutive internal concentration polarization on flux behavior in forward osmosis, J. Membr. Sci. 284 (2006) 237–247.
[26] S. Loeb, L. Titelman, E. Korngold, J. Freiman, Effect of porous support fabric on osmosis through a Loeb–Sourirajan type asymmetric membrane, J. Membr. Sci. 129 (1997) 243–249.
[27] J.R. McCutcheon, M. Elimelech, Modelling water flux in forward osmosis: implications for improved membrane design, AIChE J. 53 (2007) 1736–1744.
[28] B. Gu, D.Y. Kim, J.H. Kim, D.R. Yang, Mathematical model of flat sheet membrane modules for FO process: plate-and-frame module and spiral-wound module, J. Membr. Sci. 379 (2011) 403–415.
[29] S. Sundaramoorthy, G. Srinivasan, D.V.R. Murthy, An analytical model for spiral wound reverse osmosis membrane modules: Part I — model development and parameter estimation, Desalination 280 (2011) 403–411.
[30] A. Achilli, T.Y. Cath, A.E. Childress, Power generation with pressure retarded osmosis: an experimental and theoretical investigation, J. Membr. Sci. 343 (2009) 42–52.
[31] W.A. Phillip, J.S. Yong, M. Elimelech, Reverse draw solute permeation in forward osmosis: modeling and experiments, Environ. Sci. Technol. 44 (2010) 5170–5176.
[32] C.Y. Tang, Q. She, W.C.L. Lay, R. Wang, A.G. Fane, Coupled effects of internal concentration polarization and fouling on flux behavior of forward osmosis membranes during humic acid filtration, J. Membr. Sci. 354 (2010) 123–133.
[33] S. Zhang, K.Y. Wang, T.-S. Chung, H. Chen, Y.C. Jean, G. Amy, Well-constructed cellulose acetate membranes for forward osmosis: minimized internal concentration polarization with an ultra-thin selective layer, J. Membr. Sci. 360 (2010) 522–535.
[34] E.L. Cussler, Diffusion – Mass Transfer in Fluid Systems, 3rd ed., Cambridge University Press, Cambridge, UK, 2007.
[35] M. Park, J.J. Lee, S. Lee, J.H. Kim, Determination of a constant membrane structure parameter in forward osmosis processes, J. Membr. Sci. 375 (2011) 241–248.
[36] C.H. Tan, H.Y. Ng, Modified models to predict flux behavior in forward osmosis in consideration of external and internal concentration polarizations, J. Membr. Sci. 324 (2008) 209–219.
[37] J.R. McCutcheon, R.L. McGinnis, M. Elimelech, Desalination by ammonia–carbon dioxide forward osmosis: influence of draw and feed solution concentrations on process performance, J. Membr. Sci. 278 (2006) 114–123.
[38] S. Phuntsho, H.K. Shon, S. Vigneswaran, J. Kandasamy, S.K. Hong, S.Y. Lee, Influence of temperature and temperature difference in the performance of forward osmosis desalination process, J. Membr. Sci. 415–416 (2012) 734–744.
[39] N.T. Hancock, T.Y. Cath, Solute coupled diffusion in osmotically driven membrane processes, Environ. Sci. Technol. 43 (2009) 6769–6775.
[40] S.-M. Shim, W.-S. Kim, A numerical study on the performance prediction of forward osmosis process, J. Mech. Sci. Technol. 27 (2013) 1179–1189.
[41] E.M. Garcia-Castello, J.R. McCutcheon, M. Elimelech, Performance evaluation of sucrose concentration using forward osmosis, J. Membr. Sci. 338 (2009) 61–66.
[42] G.T. Gray, J.R. McCutcheon, M. Elimelech, Internal concentration polarization in forward osmosis: role of membrane orientation, Desalination 197 (2006) 1–8.
[43] S. Zhao, L. Zou, D. Mulcahy, Effects of membrane orientation on process performance in forward osmosis applications, J. Membr. Sci. 382 (2011) 308–315.
[44] Y. Wang, F. Wicaksana, C.Y. Tang, A.G. Fane, Direct microscopic observation of forward osmosis membrane fouling, Environ. Sci. Technol. 44 (2010) 7102–7109.
[45] S. Loeb, M.R. Bloch, Countercurrent flow osmotic processes for the production of solutions having a high osmotic pressure, Desalination 13 (1973) 207–215.
[46] H. Niemi, S. Palosaari, Flowsheet simulation of ultrafiltration and reverse osmosis processes, J. Membr. Sci. 91 (1994) 111–124.
[47] Y.-Y. Lu, Y.-D. Hu, X.-L. Zhang, L.-Y. Wu, Q.-Z. Liu, Optimum design of reverse osmosis system under different feed concentration and product specification, J. Membr. Sci. 287 (2007) 219–229.
[48] K.M. Sassi, I.M. Mujtaba, Optimal design and operation of reverse osmosis desalination process with membrane fouling, Chem. Eng. J. 171 (2011) 582–593.
[49] D. Xiao, W. Li, S. Chou, R. Wang, C.Y. Tang, A modeling investigation on optimizing the design of forward osmosis hollow fiber modules, J. Membr. Sci. 392–393 (2012) 76–87.
[50] D.L. Shaffer, L.H. Arias Chavez, M. Ben-Sasson, S. Romero-Vargas Castrillón, N. Y. Yip, M. Elimelech, Desalination and reuse of high-salinity shale gas produced water: drivers, technologies, and future directions, Environ. Sci. Technol. 47 (2013) 9569–9583.
[51] S.M. Mamisaheby, S.P. Phuntsho, H.S. Shon, F.L. Lotfi, J.K. Kim, Factors affecting the performances of forward osmosis desalination process, Proc. Eng. 44 (2012) 1449–1451.
[52] B.R. Babu, N.K. Rastogi, K.S.M.S. Raghavarao, Effect of process parameters on transmembrane flux during direct osmosis, J. Membr. Sci. 280 (2006) 185–194.
[53] S. Phuntsho, A novel fertiliser drawn forward osmosis desalination for fertigation, University of Technology, Sydney, 2012. (Ph.D. thesis).
[54] S. Phuntsho, S. Mamisahebi, T. Majeed, F. Lotfi, J.E. Kim, H.K. Shon, Assessing the major factors affecting the performances of forward osmosis and its implications on the desalination process, Chem. Eng. J. 231 (2013) 484–496.
[55] Y.C. Kim, S.-J. Park, Experimental study of a 4040 spiral-wound forward-osmosis membrane module, Environ. Sci. Technol. 45 (2011) 7737–7745.
[56] D.H. Jung, J. Lee, D.Y. Kim, Y.G. Lee, M. Park, S. Lee, D.R. Yang, J.H. Kim, Simulation of forward osmosis membrane process: effect of membrane orientation and flow direction of feed and draw solutions, Desalination 277 (2011) 83–91.
[57] A. Subramani, M. Badruzzaman, J. Oppenheimer, J.G. Jacangelo, Energy minimization strategies and renewable energy utilization for desalination: a review, Water Res. 45 (2011) 1907–1920.
[58] R. Semiat, Energy issues in desalination processes, Environ. Sci. Technol. 42 (2008) 8193–8201.
[59] C.R. Martinetti, A.E. Childress, T.Y. Cath, High recovery of concentrated RO brines using forward osmosis and membrane distillation, J. Membr. Sci. 331 (2009) 31–39.
[60] J.R. McCutcheon, R.L. McGinnis, M. Elimelech, A novel ammonia–carbon dioxide forward (direct) osmosis desalination process, Desalination 174 (2005) 1–11.
[61] R.A. Robinson, R.H. Stokes, Electrolyte Solutions, 2nd ed., Reprinted Courier Dover Publications, NY (2002) 1959.